Spatial and Diurnal Variations of Aerosol Organosulfates in Summertime Shanghai, China: Potential Influence of Photochemical Process and Anthropogenic Sulfate Pollution

Ting Yang[1], Yu Xu[1],*, Qing Ye[1], Yi-Jia Ma[1], Yu-Chen Wang[2], Jian-Zhen Yu[2], Yu-Sen Duan[3], Chen-Xi Li[1], Hong-Wei Xiao[1], Zi-Yue Li[1], Yue Zhao[1],*, Hua-Yun Xiao[1],*

[1]School of Environmental Science and Engineering, Shanghai Jiao Tong University, Shanghai 200240, China

[2]Division of Environment & Sustainability, Hong Kong University of Science & Technology, Hong Kong SAR, China

[3]Shanghai Environmental Monitoring Center, Shanghai 200235, China

*Corresponding authors

Yu Xu, e-mail: xuyu360@sjtu.edu.cn

Yue Zhao, e-mail: yuezhao20@sjtu.edu.cn

Hua-Yun Xiao, e-mail: xiaohuayun@sjtu.edu.cn

ABSTRACT:Organosulfates (OSs) are ubiquitous aerosol components with intense research over years. However, spatial and diurnal variations in OS formation in polluted atmosphere remain poorly understood. In this study, 130 OS species were quantified (or semi-quantified) in ambient fine particulate matter ($PM_{2.5}$) collected in urban and suburban Shanghai (East China) in summer 2021. Isoprene- and monoterpene-derived OSs were dominant OS groups (averaging 51% and 19% of total quantified OSs, respectively), likely indicating a large biogenic contribution to OS formation in summer. Most OSs peaked during daytime, while monoterpene-derived nitrooxy-OSs (NOS_m) increased during nighttime. Accordingly, OSs were largely produced via daytime formation processes, rather than nighttime chemistry, excepting NOS_m. Additionally, although OS formation in the urban and suburban areas exhibited similar diurnal variations, the average concentrations of biogenic and anthropogenic OSs decreased significantly from the urban site to the suburban site. Furthermore, we concretized daytime OS formation based on the interactions among OSs, ultraviolet (UV), ozone (O_3), and sulfate (SO_4^{2-}). Indeed, the concentrations of most OSs were significantly correlated with the values of $UV[O_3][SO_4^{2-}]$ during daytime in both urban and suburban Shanghai. In particular, the correlation between major OSs and $UV[O_3][SO_4^{2-}]$ was stronger than the correlation of major OSs with O_3 and SO_4^{2-}; moreover, there was no significant correlation between major OSs and UV. Thus, higher urban OS events were attributed to the enhanced photochemical processes and sulfate level in the urban area. Overall, this study provides field evidence for the influence of photochemical process and anthropogenic sulfate on OS formation and has important implications for the

47 mitigation of organic particulate pollution.

48 **KEYWORDS:** Organosulfates; Aerosols; Photooxidation; Sulfate pollution; Shanghai

1. Introduction

51   Organosulfates (OSs) are ubiquitous constituents in secondary organic aerosol

52 (SOA) and can contribute up to ~30% of organic mass in atmospheric fine particles

53 ($PM_{2.5}$) (Tolocka andTurpin 2012; Surratt et al. 2008; Hettiyadura et al. 2018). OSs

54 affect the formation, hygroscopicity, light-absorbing, and acidity of organic aerosols as

55 well as biogeochemical cycles of sulfur (Estillore et al. 2016; Riva et al. 2019; Fleming

56 et al. 2019), which are tightly associated with air quality, human health, and regional

57 climate (Ramanathan et al. 2001; Menon et al. 2008). Thus, understanding the

58 mechanisms and key influencing factors of OS formation in the ambient atmosphere is

59 of great significance for an effective assessment of environment and climate effects of

60 OSs.

61   Many laboratory studies have suggested that heterogeneous and multiphase

62 reactions involving biogenic and anthropogenic volatile organic compounds (VOCs),

63 their oxidation intermediates, and sulfate or gas-phase sulfur dioxide (SO_2) are

64 important pathways for the formation of OSs (Blair et al. 2017; Riva et al. 2016b; Ye et

65 al. 2018). For example, the formation of 2-methyltetrol sulfate ester (2-MT-OS) and 2-

66 methylglyceric acid sulfate ester (2-MGA-OS) can be attributed to the reactive uptake

67 of isoprene epoxydiols (IEPOX) and isoprene-derived hydroxymethyl-methyl-α-

68 lactone (HMML) by acidic particles, respectively (Surratt et al. 2010; Nguyen et al.

2015). The ozonolysis of α-pinene and limonene in the presence of SO_2 can contribute

to the production of monoterpene-derived OSs (e.g., $C_9H_{15}O_7S^-$ and $C_{10}H_{17}O_7S^-$) (Ye

et al. 2018). Chamber experiments by Riva et al., (Riva et al. 2015) showed that the

photooxidation of C_{10}–C_{12} alkanes is associated with the formation of aliphatic OSs.

More recently, the aliphatic OSs have been identified based on the uptake experiments

of SO_2 by oleic acid and other unsaturated fatty acids (Shang et al. 2016; Passananti et

al. 2016). In addition, the gas-phase oxidation of polycyclic aromatic hydrocarbons was

found to be an important source of aromatic OSs (Riva et al. 2015).

Furthermore, OSs have been identified in different ambient atmospheres, including

suburban, rural, urban, marine, polar, and forest areas (Kristensen andGlasius 2011;

Hettiyadura et al. 2017; Hawkins et al. 2010; Stone et al. 2012; Hettiyadura et al. 2018;

Hansen et al. 2014; Glasius et al. 2018). Owing to different levels of precursors and

atmospheric pollution, the abundance and formation pathways of OSs change

substantially in temporal and spatial scales (Wang et al. 2021; Ding et al. 2022; Jiang

et al. 2022; Nozière et al. 2010; O'brien et al. 2014). Patently, field observations are

valuable for verifying the mechanistic understanding of OS formation obtained in the

laboratory studies. The importance of atmospheric oxidants and sulfate (or SO_2) in the

OS formation was proposed in field observations according to a correlation analysis of

OSs with ozone (O_3) (or the sum of O_3 and NO_2 concentrations) and sulfate (or SO_2)

(Nguyen et al. 2014; Hettiyadura et al. 2019; Wang et al. 2018). Notably, these

observation-based studies also highlighted the role of photochemistry of OS precursors.

However, the interactions among ultraviolet (UV), O_3, and sulfate have not been well

91 investigated. In particular, few studies were performed to systematically reveal the

92 difference in the formation processes of OSs in polluted and clean areas, as well as

93 during daytime and nighttime.

94   Shanghai is a megacity in the Yangtze River Delta (YRD) region of China.

95 Locally varied ambient conditions such as O_3, SO_2, and NO_x, relative humidity (RH),

96 and aerosol acidity affect the formation of OSs significantly (Cai et al. 2020; Wang et

97 al. 2021). Here, 130 OS species were quantified (or semi-quantified) in $PM_{2.5}$ samples

98 collected in urban and suburban Shanghai in summer 2021 to investigate the relative

99 influence of photochemistry and nighttime chemistry on OS formation and their

100 linkages with anthropogenic sulfate pollution. In addition, the potential impacts of

101 aerosol acidity and aerosol liquid water (ALW) on OS formation were discussed. This

102 study can help to deepen the understanding of photochemical process and nighttime

103 chemistry of OSs in the atmosphere.

104

105 **2. Materials and Methods**

106 **2.1 Site Description and Sample Collection**

107   Ambient $PM_{2.5}$ samples were continuously collected in the urban center and

108 suburban area in Shanghai from 11 to 23 July 2021 (**Figure S1**). The sampling site in

109 the urban center is located on the roof of a building (~20 m above the ground) in the

110 Xuhui Campus of Shanghai Jiao Tong University. The site is characterized by a typical

111 urban environment with heavy traffic and dense population. The aerosol sampler in the

112 suburban area was placed on the roof of a ~20 m high building in a monitoring station

113   of Pudong Huinan. This site is closer to the coastline than the urban sampling site

114   (**Figure S1**). Thus, the suburban site is expected to be more affected by clean air mass

115   from the sea. $PM_{2.5}$ was sampled onto the prebaked (550°C for ∼8 h) quartz fiber filters

116   (8 × 10 in., Whatman) using a high-volume air sampler (HiVol 3000, Ecotech) at a flow

117   rate of 67.8 m^3 min^{-1}. The duration of each sample collection in both urban and

118   suburban areas was approximately 11 h during the daytime (8:30−19:30 LT) and 12 h

119   during the nighttime (20:00−8:00 LT). Two blank filter samples were collected at each

120   site during the campaign. A total of 50 filter samples were collected, which were stored

121   at −30°C until analysis.

122

123   **2.2 Chemical Analysis and Prediction of Aerosol Acidity and ALW**

124   A portion of the filter (~15.9 cm^2) was extracted with 3 mL methanol in an

125   ultrasonic bath for 30 min for two times. The sodium camphor sulfonate (1 ppm) was

126   spiked on the filter punches as an internal standard before extracting. The extracts

127   obtained each time were combined and filtered through a 0.22 μm Teflon syringe filter

128   (CNW Technologies GmbH) and then concentrated to 300 μL under a gentle stream of

129   ultra-high-purity nitrogen gas. Subsequently, 300 μL ultrapure water was added into the

130   concentrated samples, followed by centrifugation to get the supernatant for analysis.

131   OSs were analyzed using an Acquity UPLC (Waters, USA) coupled to a Xevo G2-XS

132   Quadrupole time-of-flight mass spectrometer (ToF-MS, Waters, USA) equipped with

133   an electrospray ionization (ESI) source operated in the negative ion mode. The

134   chromatographic conditions and analytical procedures were detailed in our recent

135   publication (Wang et al. 2021).

136   A total of 212 OSs were identified by UPLC-MS analysis, in which 130 OS species

137   were quantified (or semi-quantified) (**Table 1** and **Table S1**). The quantified (or semi-

138   quantified) species included isoprene-derived OSs (OS_i), monoterpene-derived OSs

139   (OS_m), C_2-C_3 OSs, aliphatic OSs, and aromatic OSs (Hettiyadura et al. 2019). It is worth

140   noting that most of identified OSs were semi-quantified using surrogate standards

141   because of the lack of authentic standards (Staudt et al. 2014; Hettiyadura et al. 2015).

142   The surrogate OS standards included potassium phenyl sulfate (98%, Tokyo Chemical

143   Industry), methyl sulfate (99%, Macklin), sodium octyl sulfate (95%, Sigma-Aldrich),

144   glycolic acid sulfate (artificial synthesis), lactic acid sulfate (artificial synthesis),

145   limonaketone sulfate (artificial synthesis), and α-pinene sulfate (artificial synthesis)

146   (Olson et al. 2011; Wang et al. 2017; Hettiyadura et al. 2019; Hettiyadura et al. 2017;

147   Wang et al. 2018), as detailed by our previous study (Wang et al. 2021). Considering

148   that OSs with similar structures of carbon backbone typically have similar MS

149   responses (Wang et al. 2021; Wang et al. 2017), the selection of surrogate standard for

150   a given OS was primarily based on the similarities in the carbon chain structure of the

151   standard and targeted OS species (Hettiyadura et al. 2017). Furthermore, the similarities

152   of the sulfur-containing fragment ions in the MS/MS spectra of the standard and

153   targeted OS species have also been adopted (Wang et al. 2021; Hettiyadura et al. 2019).

154   For OSs that have been reported in previous studies, MS/MS can further support their

155   structural identifications (**Table 1**). However, most of OSs without identified structural

156   information were classified and semi-quantified according to their molecular formulas

and correlation analysis with known OSs and unidentified OSs (**Sect. S1**) (Bryant et al. 2021; Hettiyadura et al. 2019). Details about the standards used for quantitative OS species as well as about the classification or identification of OSs were shown in Table 1, Table S1, and Supplementary Information (**Sect. S1**). We found that most of OSs without identified structural information in previous studies and this study had significantly lower peak intensity compared to those listed in Table 1, implying that these OS compounds have weak impact on total OS abundance in ambient aerosols. In general, the differential ionization efficiencies and fragmentation patterns in the OS measurement may introduce biases (Hettiyadura et al. 2017). Consequently, the OS species shown in Table 1 and Table S1 should not be regarded as an accurate measure of OS compounds, but a best solution in the absence of authentic OS standards (Hettiyadura et al. 2015; Hettiyadura et al. 2017; Hettiyadura et al. 2019; Wang et al. 2021). The recoveries of OS standards ranged from 84% to 94% (87%±4%). Thus, we assumed that there is a high extraction efficiency for major OS species in this study, as indicated by previous studies (Wang et al. 2021; Hettiyadura et al. 2015). Detailed data quality control was described in our recent publication (Wang et al. 2021).

The mass concentrations of organic carbon (OC) and elemental carbon (EC) were determined via an OC/EC analyzer (DRI Model 2015). The mass concentrations of OC were converted to those of organic matter (OM) using a conversion factor of 1.6 (Turpin andLim 2001; Wang et al. 2021; Wang et al. 2018). The mass concentrations of inorganic ions in PM$_{2.5}$ samples, including Na$^+$, NH$_4^+$, K$^+$, Mg^{2+}, Ca^{2+}, Cl$^-$, NO$_3^-$, and SO$_4^{2-}$, were measured using an ion chromatograph system (ICS-5000+, Thermo, USA).

179   A thermodynamic model (ISORROPIA-II) was used to predict the mass

180   concentration of ALW and pH (Guo et al. 2015; Hennigan et al. 2015). The model was

181   operated with particle-phase concentrations of Na^+, SO_4^{2-}, NH_4^+, NO_3^-, Cl^-, Ca^{2+}, K^+,

182   and Mg^{2+}, as well as ambient temperature (T) and RH as the inputs. Moreover, the

183   forward mode with the thermodynamically metastable state was selected. The detailed

184   descriptions on ALW and pH predictions were shown in our previous studies (Wang et

185   al. 2021; Xu et al. 2020). In particular, we compared different outputs of the pH values

186   calculated by ISORROPIA-II between the cases with and without considering OSs as

187   additional sulfates to investigate potential impact of OSs on pH prediction (Riva et al.

188   2019). The pH values predicted from these two cases (2.55 ± 0.93 vs 2.65 ± 0.94 at the

189   urban site and 2.17 ± 0.68 vs 2.23 ± 0.74 at the suburban site) have an insignificant

190   difference. Thus, OSs were expected to have a considerably small contribution to pH

191   prediction in this study.

192

193   **2.3. Auxiliary Data and Data Analysis**

194   The transport trajectories of air masses arriving at the sampling sites during the

195   sampling period were created using the database of NOAA's Air Resources Laboratory

196   (NOAA's Air Resources Laboratory, USA) and MeteoInfoMap software coupled with

197   TrajStat program (Chinese Academy of Meteorological Sciences, China). The data of

198   T, RH, wind speed, and UV irradiation as well as the concentrations of NO, NO_2, O_3,

199   SO_2, and $PM_{2.5}$ at the urban and suburban sites were obtained from the environmental

200   monitoring stations of Xuhui (~4 km away from the sampling site) and Pudong Huinan

201   (~10 m away from the sampling site), respectively. The ventilation coefficient (VC) can

202   be used to characterize the state of atmospheric dilution in pollutant concentrations

203   (Gani et al. 2019). The VC value can be expressed as a product of wind speed and

204   planetary boundary layer height (PBLH).

205

206   **3. Results and Discussion**

207   **3.1. Molecular compositions and concentrations of OSs**

208   The mass concentrations and mass fractions of the OS species in $PM_{2.5}$ collected

209   in Shanghai were shown in **Figure 1**, with a focus on their spatial and diurnal

210   differences. On average, isoprene-derived OSs (i.e., OS_i) were the dominant

211   components at both urban and suburban sites (**Figures 1a,d**), which accounted for 53.9

212    $\pm$ 0.1% and 48.1 $\pm$ 0.1% of the total OS masses, respectively. The mass fractions and

213   concentrations of $C_5H_{11}O_7S^-$ were the highest among all kinds of OS_i. In contrast, OS_i

214   containing nitrogen atoms only accounted for a small proportion of OS_i in both urban

215   and suburban areas (**Figures 1a,d** and **Table S2**). Monoterpene-derived OSs (OS_m)

216   were the second most abundant OS components, whose concentrations averaged 30.6

217    $\pm$ 46.4 ng m^{-3} and 19.3 $\pm$ 25.7 ng m^{-3} in the urban and suburban areas, respectively.

218   Moreover, the abundance of OS_m was also less controlled by nitrogen-containing OS_m.

219   On average, the OS species with two or three carbon atoms (C_2-C_3 OSs) and

220   anthropogenic OSs (OS_a) together contributed to 26.8% and 33.1% of total OS

221   concentrations in the urban and suburban areas, respectively (**Figures 1a,d** and **Table**

222   **S3**). A similar pattern in the relative abundance of different groups of OSs was also

223 observed at the same sites in summer 2020 (**Figure S2**). The predominance of OS_i was

224 well documented by many previous observations in Beijing, China (Wang et al. 2018),

225 Guangzhou, China (Bryant et al. 2021), and Atlanta, Georgia, USA (Hettiyadura et al.

226 2019), Hong Kong, China (Wang et al. 2022), Copenhagen, Denmark (Nguyen et al.

227 2014), Centreville, AL, USA (Hettiyadura et al. 2017), Zion, Illinois, USA (Hughes et

228 al. 2021). A reasonable explanation for these cases is that there is a large biogenic

229 emission of isoprene, particularly during summer days with higher temperature than in

230 other seasons (Bryant et al. 2021). Interestingly, we found that the mass concentrations

231 of all types of OSs (i.e., total OS_i, OS_m, C_2-C_3 OSs, and OS_a) tended to decrease from

232 the urban area to the suburban area. This spatial difference in OS concentrations can be

233 attributed to varied atmospheric oxidation capacity and aerosol properties (e.g., sulfate,

234 acidity, and ALW) (Wang et al. 2021), which will be discussed in detail below.

235   **Table S4** gives an overview of OSs in $PM_{2.5}$ in different regions around the world.

236 The concentrations of total OSs in our study (more than 102.3 ng m^{-3}) were higher than

237 those in Copenhagen, Denmark (75.7 ng m^{-3}) (Nguyen et al. 2014), and Beijing, China

238 (27.4 ng m^{-3}) (Wang et al. 2018). However, the OSs showed a lower concentration in

239 Shanghai compared to the observations in Guangzhou (486.4 ng m^{-3}) (Wang et al. 2022)

240 and Atlanta, USA (Hettiyadura et al. 2019) (1249.4 ng m^{-3}). The concentrations of OS_i

241 in this study were lower than those observed in summertime Atlanta, USA (1123.0 ng

242 m^{-3}) (Hettiyadura et al. 2019), Guangzhou, China (460.2 ng m^{-3}) (Wang et al. 2022),

243 and Hongkong, China (163.2 ng m^{-3}) (Wang et al. 2022), but higher than Copenhagen,

244 Denmark (11.3 ng m^{-3}) (Nguyen et al. 2014). For OS_m and C_2-C_3 OSs, their

245   concentrations also showed a variable range in different regions (**Table S4**). The

246   concentrations of OS_a in this study were much higher than those in previous

247   observations (Hettiyadura et al. 2017; Kanellopoulos et al. 2022), which is likely

248   explained by more OS_a species being quantified or higher air pollution level in this study.

249   It should be noted that these spatial comparisons for OS levels mentioned above

250   involved more or less uncertainty due to the lack of authentic standards for precise

251   quantification of OSs. However, our semi-quantitative data provides at least literature

252   reference for future research on these OSs. At the same study site, the abundances of

253   biogenic OSs (OS_i + OS_m) were typically higher than those of other types of OSs,

254   particularly during the summertime when vegetation grows vigorously (**Table S4**).

255   Thus, the yield of summertime OSs in the investigated areas largely depends on the

256   emission level of biogenic VOCs and the air pollution status.

257   We found that the contributions of total OSs to OM were $1.3 \pm 0.5\%$ and $1.9 \pm 0.5\%$

258   at urban and suburban sites in summer 2021, respectively. These proportions of total

259   OSs in OM were larger than those observed in Beijing, China (0.3%) (Wang et al. 2018)

260   and Centreville, USA (0.2%) (Hettiyadura et al. 2017). However, significant higher

261   contribution of total OSs to OM was observed in Atlanta, USA (10.3%) (Hettiyadura et

262   al. 2019) where the formation of OSs was dominated by the oxidation of biogenic VOCs.

263   In particular, total OSs contributed to $1.2 \pm 0.8\%$ of OM in summer 2015 and $1.1 \pm 0.8\%$

264   of OM in summer 2019 in urban Shanghai (Wang et al. 2021). Thus, although

265   anthropogenic emission reduction has been vigorously promoted by the local

266   government in recent years (Guo et al. 2022; Pei et al. 2022) , the contribution of SOA

267   to OM in Shanghai has not decreased significantly as expected (Wang et al. 2021).

268   **Figures 1b,e** show diurnal differences in the mass concentrations and mass

269   fractions of the OS components in $PM_{2.5}$ collected at the urban site. The OS_i was the

270   dominant sulfur-containing species regardless of in daytime and nighttime. However,

271   the concentrations of OS_i exhibited a significant decrease from the daytime (117.8 ±

272   148.1 ng m^{-3}) to the nighttime (43.9 ± 62.0 ng m^{-3}), except for isoprene-derived

273   nitrooxyorganosulfates (NOS_i). Moreover, the variations in OS_i mass concentrations

274   ($\sim$2 times) were much larger than those in OS_i mass fractions (< 1.2 times). These

275   results indicate that the production of major OS_i (e.g., $C_5H_{11}O_7S^-$, $C_5H_9O_7S^-$ and

276     $C_5H_7O_7S^-$) was weakened during the nighttime. In contrast, the higher concentration

277   for these OS_i in the daytime can be attributed to the increased levels of precursors (e.g.,

278   isoprene) (Bryant et al. 2021) and oxidants (e.g., O_3) (**Table S5**) as well as the strong

279   photochemistry in the daytime. Although the average fraction of NOS_i was higher in

280   the nighttime than in the daytime, their concentration was similar between the daytime

281   and nighttime. This is because that several special NOS_i (e.g., $C_5H_{10}NO_9S^-$,

282     $C_5H_8NO_{10}S^-$, $C_4H_8NO_7S^-$, and $C_5H_8NO_7S^-$) peaked in the daytime, although

283     $C_5H_9N_2O_{11}S^-$ showed maximum in the nighttime (**Table S2**). Previous laboratory

284   studies have suggested that the formation of $C_5H_{10}NO_9S^-$ is mainly related to •OH

285   oxidation processes (Hamilton et al. 2021). Thus, a strong photochemical oxidation

286   during daytime can be responsible for the increases in concentrations of these NOS_i

287   (particularly $C_5H_{10}NO_9S^-$) from the nighttime to the daytime. Overall, the diurnal

288   variations of other OSs including OS_m, C_2-C_3 OSs, and OS_a were similar to that of OS_i,

with a higher level in the daytime than in the nighttime excepting for NOSs (**Figure 1** and **Tables S2** and **S3**). It is noteworthy that the fractions and concentrations of monoterpene-derived NOSs (NOS_m) were higher in the nighttime than in the daytime (**Table S2**). This case can be attributed to NO_3•-related nighttime chemistry (Wang et al. 2018). Thus, these findings further emphasize the importance of photochemistry for daytime OS formation and nighttime chemistry for NOS (in particular NOS_m) formation in urban Shanghai.

The concentrations of various types of OSs at the suburban site were lower than those at the urban site in both daytime and nighttime (**Figures 1b,c**). However, the characteristics of diurnal difference in various OSs at the suburban site were similar to those observed at the urban site, which showed a substantially higher OS level in the daytime. A similar case was also found in Beijing in 2016 (Wang et al. 2018) and Shanghai in 2017 (Cai et al. 2020). Clearly, the aerosol OS abundance in Shanghai was mainly controlled by the OS formation process in the daytime rather than in the nighttime.

3.2. Time series of the major OSs

Figures 2a-2h compare the time series of the major OS species and inorganic ions in $PM_{2.5}$ collected at urban and suburban sites. The OS_i concentrations peaked during daytime on July 11 and 12, with maximum values of 479.8 ng m^{-3} and 309.5 ng m^{-3} at urban and suburban sites, respectively. Owing to the high proportion of OS_i in total OSs, total OS concentrations also showed maximum values during July 11 and 12. The mass

311   concentrations of total OSs, OS$_i$, and C$_5$H$_{11}$O$_7$S$^-$ (a major OS$_i$ component) decreased

312   from July 11 to July 14 (period A; i.e., relatively polluted period) in both urban and

313   suburban areas, whereas their concentrations exhibited a quite small fluctuation after

314   July 14 (period B; i.e., clean period). As a result, the mean concentrations of total OSs

315   and OS$_i$ were ~4 times higher in the period A than in the period B. The temporal

316   variations in the concentrations of OS$_m$, C$_8$H$_{13}$O$_7$S$^-$ (a major component of OS$_m$)

317   (Schindelka et al. 2013), OS$_a$, and C$_2$-C$_3$ OSs were similar to those of total OSs and OS$_i$.

318   However, the dissimilarities in the diurnal variations of OSs in period A and period B

319   suggest that the sources or levels of precursors and oxidants associated with OS

320   formation differed between these two periods. This consideration was further supported

321   by decreasing O$_3$ and NO$_2$ levels from period A to period B (**Table S5** and **Figures 2i,j**).

322   Sulfate showed a temporal variation similar to total OSs, OS$_i$, and OS$_m$

323   concentrations in most days (**Figures 2g,h**). We observed several abnormally high

324   sulfate events during period B (from the evening of the 17th to 18th). The transport

325   distance of air mass on July 18 was found to be shorter than that in other days (**Figure**

326   **S3**); moreover, VC value was lower on July 18 than on other days (**Figure S4**). Thus,

327   this high sulfate case can be partly attributed to the special meteorological conditions

328   on July 18. In general, sulfate concentrations showed a strong correlation with total OSs,

329   OS$_i$, and OS$_m$ concentrations at both sites ($P < 0.01$, $r = 0.76–0.78$). These results

330   indicate that the abundances of OSs in these two study areas were tightly associated

331   with sulfate-related particle-phase chemistry (Surratt et al. 2008).

332   The concentrations of total OSs, OS$_i$, and OS$_m$ exhibited a distinct diurnal

333   variation during period A at both sites, with a higher concentration in the daytime. The

334   diurnal variation pattern of OSs was similar to those of O_3 and sulfate. These findings

335   imply an important role of atmospheric oxidation capacity and sulfate in daytime OS

336   formation. Exceptionally, although a clear diurnal pattern was also observed for NOS_m,

337   their concentrations peaked in the nighttime, suggesting that the formation of NOS_m

338   was highly affected by the $NO_3\bullet$-related nighttime chemistry (Iinuma et al. 2007;

339   Surratt et al. 2008). In the period B, the concentrations of various OSs showed a weak

340   diurnal variation, with a slightly higher level in the daytime.

341   As mentioned above, the ambient levels of oxidants (e.g, O_3 and NO_2) and sulfates

342   showed a significant difference in period A and period B, which were tightly associated

343   with the formation of OSs (Wang et al. 2021). Cluster analysis of backward trajectories

344   showed that air masses arriving at both urban and suburban sites in the period A mainly

345   originated from the continental region, with significant influences of anthropogenic

346   emissions (e.g., NO_x and SO_2) from southern YRD. Furthermore, considering the

347   distinct and similar diurnal variation of O_3, NO_2, SO_2, sulfate, and OSs during period A

348   at both sites, aerosol OSs can be assumed to be mainly formed in local areas. In contrast,

349   these two sampling sites were primarily affected by air masses transported from the

350   East China Sea in the period B. Moreover, the average VC value in the period A was

351   two times lower than that in the period B (**Table S5**), implying relatively weaker

352   diffusion and dilution of air pollutants in the period A. These factors can be partly

353   responsible for the higher oxidant and sulfate concentrations in the period A than in the

354   period B. Similarly, since the suburban site is closer to the East China Sea with a

decreased influence from anthropogenic emissions (**Figure 3**), the levels of O_3, NO_x, and sulfate were higher at the urban site than at the suburban site (**Figure 2** and **Table S5**). The differences in the concentration of oxidants and sulfate might provide an explanation for the difference in the concentrations of OSs between periods A and B as well as between urban and suburban sites.

3.3. Formation mechanisms of OSs

3.3.1 Isoprene-derived OSs

Previous laboratory studies have suggested that isoprene can react with •OH to form IEPOX in the gas phase under low NO_x conditions (Fabien et al. 2009). In the daytime, ambient O_3 can be rapidly photolyzed to generate •OH under the influence of UV (Kourtchev et al. 2015). Thus, O_3 and UV could serve as a proxy of •OH. Considering a significant role of photochemistry and sulfate-related heterogeneous chemistry in the formation of OSs, OS_i production is expected to be closely associated with isoprene, O_3, UV, and sulfate. Specifically, the simplified pathways leading to the formation of OS_i in the atmosphere can be derived as follows.

$$O_3 + hv \rightarrow O(^1D) + O_2 \qquad J_{O_3} \quad (1)$$

$$O(^1D) + H_2O \rightarrow 2 \text{ •OH} \qquad k_1 \quad (2)$$

$$O(^1D) + M \rightarrow O(^3P) + M \qquad k_2 \quad (3)$$

$$\text{Isoprene} + \text{•OH} \rightarrow X \qquad k_3 \quad (4)$$

$$X + SO_4^{2-} \rightarrow OS_i \qquad k_4 \quad (5)$$
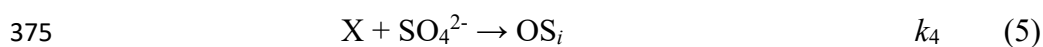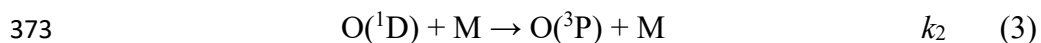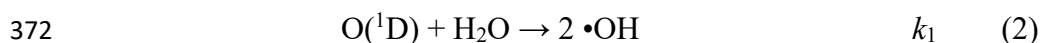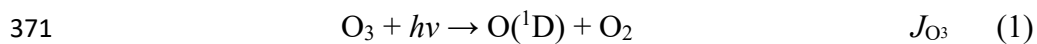
Where J_{O_3} is the photolysis rate constant, k_{1-4} is the second-order rate coefficient, M is

377   N_2 or O_2, and X represents the potential products (e.g., IEPOX and HMML) of isoprene

378   oxidation by •OH.

379   Assuming the concentrations of $O(^1D)$ and •OH are in the steady state, we can

380   derive the following equations (H. andSeinfeld 2016).

381
$$[O(^1D)] = \frac{J_{O_3}[O_3]}{k_1[H_2O] + k_2[M]} \qquad (6)$$

382
$$[\bullet OH] = 2\tau_{OH}k_1[O(^1D)][H_2O] \qquad (7)$$

383   Where τ_{OH} is the average lifetime of •OH. In general, J_{O_3} is linearly dependent on the

384   UV radiation, i.e., $J_{O_3} = \varphi UV$, where φ is the slope of the linear fitting between J_{O_3} and

385   UV radiation (Li et al. 2022). Combining equation (6) and (7), the steady-state •OH

386   concentration can be expressed as:

387
$$[\bullet OH] = \frac{2\tau_{OH}k_1[H_2O]J_{O_3}[O_3]}{k_1[H_2O] + k_2[M]} = \alpha\varphi\tau_{OH}UV[O_3] \qquad (8)$$

388
$$\alpha = \frac{2k_1[H_2O]}{k_1[H_2O] + k_2[M]} \qquad (9)$$

389   Also, assuming a steady-state to the oxygenated organic intermediates (i.e., X),

390   we can derive:

391
$$[X] = k_3\tau_X[Isoprene][OH] = \alpha\varphi k_3\tau_X\tau_{OH}[Isoprene]UV[O_3] \qquad (10)$$

392   Where τ_X is the average lifetime of X in the atmosphere.

393   During the strong formation of OS_i via the heterogeneous reactions of X on acidic

394   sulfate, the change in the abundance of OS_i is expected to be proportional to its

395   formation rate:

396
$$\frac{d[OS_i]}{dt} \propto k_4[SO_4^{2-}][X] \propto \alpha\varphi k_3 k_4 \tau_X \tau_{OH}[Isoprene]UV[O_3][SO_4^{2-}] \qquad (11)$$

397   It should be noted that the above equations are derived based on the assumption

398   that the reaction between $O(^1D)$ and H_2O is a major source of summertime •OH in the

399   studied areas. Given that a linear relationship was observed between atmospheric •OH

400   and $J_{O(^1D)}$ in different atmospheres (Stone et al., 2012), such an assumption seems to

401   be reasonable. When isoprene is in a steady state in the atmosphere, OS_i production is

402   expected to be proportional to the product of O_3, UV, and sulfate.

403    $$\frac{d[OS_i]}{dt} \propto UV[O_3][SO_4^{2-}] \tag{12}$$

404   It should be noted that equation (12) did not consider the influences of aerosol

405   acidity, ALW, and other factors (e.g., •OH production from the photolysis of nitrous

406   acid and aldehydes during the daytime). However, the deduction can at least suggest

407   that the secondary production of OS_i is positively correlated with the value of

408    $UV[O_3][SO_4^{2-}]$. Indeed, the concentrations of daytime OS_i and major OS_i species

409   showed a linear positive relationship with the value of $UV[O_3][SO_4^{2-}]$ at both urban and

410   suburban sites ($r = 0.84$–0.92, $P < 0.01$) (**Figure 4a-c**). We found that the correlation

411   between major OS_i species and $UV[O_3][SO_4^{2-}]$ was stronger than the correlation of

412   major OS_i species with O_3 and SO_4^{2-} ($r < 0.82$, $P < 0.01$); moreover, there was no

413   significant correlation between major OSs and UV ($P > 0.05$). Thus, our results provide

414   field evidence that the formation of daytime OS_i in these two study areas was mainly

415   controlled by •OH oxidation of isoprene; moreover, the higher concentration of OS_i in

416   the urban area can be attributed to the stronger atmospheric oxidation capacity (i.e.,

417   higher $UV[O_3]$ value) and more serious anthropogenic sulfate pollution (particularly

418   during period A). We also observed that the OS concentrations did not significantly

419   increase in several high sulfate events in the period B. One possible explanation is that

420   these abnormal high sulfate events resulted in excessive SO_4^{2-} in the formation of OSs.

421   2-MT-OS and 2-MGA-OS have been identified as important tracers of isoprene-

422   derived SOA (Hettiyadura et al. 2019; Cai et al. 2020). During isoprene oxidation by

423   •OH, these two OS species are produced under low (i.e., IEPOX pathway) and high

424   (i.e., HMML or methacrylic acid epoxide (MAE) pathways) NO_x conditions,

425   respectively (Surratt et al. 2010; Nguyen et al. 2015). The ratios of 2-MT-OS

426   concentration to 2-MGA-OS concentration in the daytime were 9.7 ± 3.1 and $12.1 \pm$

427   5.5 at urban and suburban sites, respectively (**Figure S5b**). A 2-MT-OS/2-MGA-OS

428   ratio of larger than 1 was also found in observations in summer 2020 (**Figure S5a**),

429   suggesting low NO_x channel dominated the formation of daytime OS_i in the two study

430   areas. This finding was similar to previous observations in Beijing (3.2) (Wang et al.

431   2020) and Guangzhou (7.6) (Bryant et al. 2021). Other abundant OS_i compounds

432   including $C_5H_7O_7S^-$, $C_4H_7O_6S^-$, and $C_5H_9O_7S^-$ can be produced by the photooxidation

433   of isoprene, heterogeneous oxidative aging of 2-MT-OS, or sulfate radical-initiated

434   reaction with methacrolein and methyl vinyl ketone in the aqueous phase (Schindelka

435   et al. 2013; Wach et al. 2019; Hettiyadura et al. 2015). These OSs showed strong

436   correlations ($r = 0.74–0.90$, $P < 0.01$) with $UV[O_3][SO_4^{2-}]$, which further highlights the

437   significance of the photochemistry in OS_i formation.

438   In the nighttime, the formation •OH can be primarily attributed to the reactions of

439   olefins and O_3 (Paulson andOrlando 1996). As shown in **Figures 4d-f**, total OS_i and

440   major OS_i compounds were significantly correlated with the product of O_3 and SO_4^{2-}

441   concentrations ($P < 0.01$, $r = 0.96–0.98$). Since the nighttime oxidant level (including

442   O_3 and •OH) was substantially lower than that in the daytime (**Table S5**), the production

443   of OS_i was weakened in the nighttime (**Table S2**). It is interesting to note the 2-MT-

444   OS/2-MGA-OS mean ratio in the nighttime was 13.1–15.0 (**Figure S5(b)**), significantly

445   higher than the mean ratio (9.7–12.1) in the daytime, indicating that the IEPOX

446   pathway may be a potential mechanism to generate OS_i in the nighttime. Another

447   possible explanation for the decreased OS concentration in the nighttime is that these

448   OSs were mainly formed during the daytime, but had a lower abundance in the

449   nighttime due to deposition and weak nighttime formation. Namely, considering the

450   strong diffusion effect during the daytime and the weak diffusion effect at the nighttime

451   (**Figure S4**), the nighttime OSs may be partially derived from OSs formed via

452   photochemical processes during the daytime. This is because the enhanced diffusion

453   effect during the daytime can result in a decrease in the amount of OS produced during

454   the daytime to deposit into the nighttime.

455   Furthermore, $NO_3\bullet$ chemistry in the nighttime was another possible pathway to

456   form OS_i, particularly NOSs. The nighttime NOS concentration was linearly correlated

457   with the product of NO_2 and O_3 ($[NO_2][O_3]$, i.e., a proxy of $NO_3\bullet$) (**Figure S6**).

458   Interestingly, most of NOS_i (e.g., $C_5H_{10}NO_9S^-$, $C_5H_8NO_{10}S^-$, $C_4H_8NO_7S^-$, and

459    $C_5H_8NO_7S^-$) have higher concentrations in the daytime, excepting for $C_5H_9N_2O_{11}S^-$.

460   Thus, although nighttime $NO_3\bullet$ chemistry was important, the NOS_i formed via

461   photochemistry under the influence of NO_x in the daytime was still dominant

462   contributors to total NOS_i in our study areas. Regarding $C_5H_9N_2O_{11}S^-$, its formation

463   pathway is mainly the $NO_3\bullet$ oxidation of $C_5H_9NO_5$ as illustrated in **Figure S7**

464   (Hamilton et al. 2021). Accordingly, the abundance of $C_5H_9N_2O_{11}S^-$ peaked during the

465   nighttime (**Figure S8**). It should be pointed out that the •OH oxidation of $C_5H_9NO_5$ can

466   also contribute to the production of $C_5H_{10}NO_9S^-$ (**Figure S7**). Clearly, this mechanism

467   can be responsible for the higher $C_5H_{10}NO_9S^-$ concentrations in the daytime as

468   mentioned above. In general, increased OS_i level in the daytime demonstrated that the

469   formation of OS_i in urban and suburban areas was largely controlled by photooxidation

470   of isoprene in the presence of sulfate in the daytime, rather than nighttime NO_3•

471   chemistry. Moreover, a decrease in average OS_i level from the urban area to the

472   suburban area can be explained by the weakened photooxidation of isoprene and the

473   decreased anthropogenic sulfate pollution (particularly in the relatively polluted period).

474

475   **3.3.2 Monoterpene-derived OSs**

476   The concentrations of the most abundant OS_m species ($C_{10}H_{15}O_7S^-$ and $C_8H_{13}O_7S^-$)

477   showed a strong correlation with the value of $UV[O_3][SO_4^{2-}]$ (and $UV[O_3][SO_2]$) in the

478   daytime at both urban and suburban sites ($r = 0.82$–0.86, $P < 0.01$), indicating that the

479   photooxidation of monoterpenes was a significant source for OS_m. Previous studies also

480   demonstrated that $C_{10}H_{15}O_7S^-$ can be produced through the photooxidation of

481   monoterpenes or sulfate radical reaction with α-pinene (Surratt et al. 2008; Nozière et

482   al. 2010).

483   In the nighttime, the concentrations of nitrogen-free OS_m species decreased

484   significantly with a decrease in the O_3 levels (Wang et al. 2020). However, NOS_m

485   species increased in concentration in the nighttime and showed a significant correlation

486   with the value of $[O_3][NO_2]$ (the proxy of NO_3•, as mentioned above) ($r = 0.90$–0.95, P

487   < 0.01). Accordingly, nighttime $NO_3\bullet$ chemistry exerted a significant influence on the

488   abundance of NOS_m in these study areas. A study by Hamilton et al., (Hamilton et al.

489   2021) has reported that $NO_3\bullet$ chemistry plays an important role in the production of

490   NOS_m. However, the overall lower OS_m level in the nighttime (**Table S2**) suggests that

491   daytime OS_m production via monoterpenes photooxidation was still the dominant

492   contributor to total OS_m throughout the day. Although several filed studies have

493   reported the abundance of various NOS_m (e.g., $C_{10}H_{16}NO_7S^-$ and $C_9H_{14}NO_8S^-$) (Wang

494   et al. 2018; Bryant et al. 2021; Cai et al. 2020), their structures, formation mechanisms,

495   and relevant diurnal variations remain large uncertainties, which need to be deeply

496   explored in the future research.

497

498   **3.3.3 C_2-C_3 and anthropogenic OSs**

499   The OS species with two or three carbon atoms (C_2-C_3 OSs) are generally

500   considered to originate from both biogenic and anthropogenic emissions (Wang et al.

501   2020). The abundant C_2-C_3 OS species, including $C_2H_3O_6S^-$ (glycolic acid sulfate;

502   GAS), $C_3H_5O_5S^-$ (hydroxyacetone sulfate; HAS), and $C_3H_5O_6S^-$ (lactic acid sulfate;

503   LAS), were significantly correlated with the values of $UV[O_3][SO_4^{2-}]$ in the daytime at

504   both urban and suburban sites ($r = 0.79$–0.91, $P < 0.01$), indicating that the

505   photochemical processes largely contributed to the formation of C_2-C_3 OSs. Recently,

506   the heterogeneous $\bullet$OH oxidation of particulate 2-MT-OS has been shown to generate

507   a series of C_2-C_3 OSs (e.g., $C_2H_3O_6S^-$, $C_3H_5O_6S^-$, and $C_2H_3O_5S^-$) (Chen et al. 2020).

508   Moreover, $C_3H_5O_4S^-$ and $C_3H_7O_5S^-$ have previously been reported to be produced by

509   the photooxidation of diesel vehicle exhausts (Blair et al. 2017).

510   Most of the quantified OS_a compounds, including $C_{13}H_{25}O_5S^-$, $C_9H_{15}O_7S^-$,

511    $C_8H_{17}O_4S^-$, benzyl sulfate ($C_7H_7O_4S^-$), phenyl sulfate ($C_6H_5O_4S^-$), as well as

512    $C_6H_9O_6S^-$, $C_5H_7O_6S^-$, and $C_4H_7O_4S^-$, exhibited a strong correlation ($P < 0.01$) with the

513   values of $UV[O_3][SO_4^{2-}]$ in the daytime. $C_{13}H_{25}O_5S^-$ has been detected in diesel exhaust

514   (Cui et al. 2019), which is the homologous compound of $C_{12}H_{23}O_5S^-$ produced from

515   dodecane photooxidation (Riva et al. 2016b). A chamber study has detected $C_9H_{15}O_7S^-$

516   in decalin SOA and speculated that it was produced via •OH oxidation of a C_9-carbonyl

517   hydroperoxide ($C_9H_{16}O_3$) and subsequent reaction on acidic sulfate aerosols (Riva et al.

518   2016b). In addition, photooxidation of diesel fuel vapor in the presence of SO_2 has been

519   suggested to be an important source of $C_6H_9O_6S^-$, $C_5H_7O_6S^-$, and $C_4H_7O_4S^-$ species

520   (Blair et al. 2017). The formation of $C_7H_7O_4S^-$ and $C_6H_5O_4S^-$ can also be attributed to

521   the photooxidation of naphthalene and 2-methylnaphthalene (Riva et al. 2015).

522   We note that the concentrations of most of C_2-C_3 OS and OS_a species decreased

523   significantly from the daytime to the nighttime (**Table S2** and **Table S3**). As discussed

524   above, the OSs observed in the nighttime may partially come from the OSs generated

525   during the daytime. Thus, the deposition effect from the daytime to the nighttime was

526   an important factor controlling nighttime levels of C_2-C_3 OSs and OS_a. In addition, the

527   nighttime gas-phase oxidation process was also likely associated with C_2-C_3 and

528   anthropogenic OS formation at both urban and suburban sites, as suggested by the

529   significant correlations of C_2-C_3 OSs and OS_a with O_3 and $[O_3][NO_2]$ in the nighttime

530   ($r = 0.89$–0.91, $P < 0.01$). Overall, these results further highlight the importance of

531   photochemistry in controlling the all-day abundance of OSs, as discussed earlier.

532

3.3.4 The effects of ALW and pH on OS formation

534   We have demonstrated that the atmospheric oxidation capacity (e.g., UV[O_3] and

535   [O_3 + NO_2]), sulfate pollution, and nighttime $NO_3\bullet$ chemistry exerted considerable

536   influences on the formation of OSs in both urban and suburban areas. In addition,

537   laboratory and field studies have suggested that aerosol properties including acidity and

538   ALW also play important roles in OS formation (Iinuma et al. 2007; Surratt et al. 2007b;

539   Wang et al. 2020; Wang et al. 2018; 2022). The aerosol pH in Shanghai in summer

540   averaged 2.7 ± 0.9 and 2.2 ± 0.7 in urban and suburban areas, respectively. The mean

541   pH value was similar to that in northern China (summer) (Ding et al. 2019; Wang et al.

542   2018), but higher than that in the Pearl River Delta (PRD) region (Fu et al. 2015). In

543   this study, only the 2-MT-OS concentration showed an evident negative correlation with

544   the pH value ($r = 0.58$, $P < 0.05$), suggesting the aerosol acidity is not a limiting factor

545   for the formation of most OS species.

546   A positive correlation was observed between the concentrations of OSs and ALW

547   only in the urban area during both daytime and nighttime (**Figure 5**), consistent with

548   our previous observations in urban Shanghai (Wang et al. 2021). It is interesting to note

549   that although higher ALW concentrations and lower pH values were observed at the

550   suburban site, the OS concentrations were significantly higher at the urban site (**Table**

551   **S5**). This result further confirms that atmospheric oxidation capacity and sulfate

552   pollution level governed the formation of OSs in urban and suburban Shanghai

553   (particularly in the relatively polluted period), though ALW and aerosol acidity also

554   played a role. Therefore, a synergistic regulation of atmospheric oxidation capacity and

555   anthropogenic SO_2 emissions would be important for the mitigation of OS and SOA

556   pollution in the megacity Shanghai.

557

4. Conclusions

559   We investigated the spatial and diurnal variations of aerosol OS formation in

560   Shanghai in summer. Isoprene- and monoterpene-derived OSs were found to be the

561   dominant OS groups during the entire sampling campaign, likely suggesting that the

562   formation of OSs was largely controlled by biogenic VOCs. Most OSs decreased from

563   the daytime to the nighttime, while NOS_m peaked during nighttime. These findings

564   suggested that OSs were mainly produced via daytime formation processes in both

565   urban and suburban areas, excepting NOS_m. Moreover, the average abundance of

566   various types of OSs showed a decrease trend from the urban area to the suburban area,

567   which can be explained by weakened atmospheric oxidation capacity and sulfate

568   pollution in the suburban area (primarily in the relatively polluted period). Further,

569   daytime OS formation was concretized according to the interactions among OSs, UV,

570   O_3, and SO_4^{2-}, suggesting that the concentrations of most OSs were significantly

571   correlated with the values of $UV[O_3][SO_4^{2-}]$ during daytime in both urban and suburban

572   Shanghai. We concluded that an enhancement in the photochemical process and sulfate

573   level can exacerbate OS pollution in the urban area. These findings were summarized

574   in a diagram (**Figure 6**). Generally, our study not only deepens the understanding about

the importance of photochemical process and anthropogenic sulfate pollution in controlling OS formation but also provides potential management strategies to decrease the abundance of particulate OSs.

Data availability

The data presented in this work are available upon request from the corresponding authors.

Supplement

The supplement related to this article is available online.

Competing interests

The authors declare no competing financial interest.

Author contributions. YZ, H-Y.X, and YX designed the study; TY, QY and Y-J.M performed field measurements; TY performed chemical analysis; YX, TY, and YZ performed data analysis; YX and TY wrote the original manuscript; and YX, YZ, Y-C.W, J-Z.Y, Y-S.D, C-X.L, H-W.X, and Z-Y.L reviewed and edited the manuscript.

Acknowledgements

This study was supported by the National Natural Science Foundation of China (grant 22022607), the Program for Professor of Special Appointment (Eastern Scholar) at

597 Shanghai Institutions of Higher Learning, the Shanghai Sailing Program (grant

598 22YF1418700), the Shanghai Pujiang Program (grant 20PJ1407600), and the National

599 Natural Science Foundation of China (grant 42005090).

600

601 **Review statement.** This paper was edited by Jason Surratt and reviewed by two

602 anonymous referees.

603

604

605 **References**

606 Berndt, T., Richters, S., Jokinen, T., Hyttinen, N., Kurten, T., Otkjaer, R. V., Kjaergaard,

607   H. G., Stratmann, F., Herrmann, H., Sipila, M., Kulmala, M., and Ehn, M.:

608   Hydroxyl radical-induced formation of highly oxidized organic compounds,

609   Nat. Commun., 7, 13677, 10.1038/ncomms13677, 2016.

610 Blair, S. L., MacMillan, A. C., Drozd, G. T., Goldstein, A. H., Chu, R. K., Pasa-Tolic,

611   L., Shaw, J. B., Tolic, N., Lin, P., Laskin, J., Laskin, A., and Nizkorodov, S. A.:

612   Molecular Characterization of Organosulfur Compounds in Biodiesel and

613   Diesel Fuel Secondary Organic Aerosol, Environ. Sci. Technol., 51, 119-127,

614   10.1021/acs.est.6b03304, 2017.

615 Bryant, D. J., Elzein, A., Newland, M., White, E., Swift, S., Watkins, A., Deng, W.,

616   Song, W., Wang, S., Zhang, Y., Wang, X., Rickard, A. R., and Hamilton, J. F.:

617   Importance of Oxidants and Temperature in the Formation of Biogenic

618   Organosulfates and Nitrooxy Organosulfates, ACS Earth Space Chem., 5, 2291-

2306, 10.1021/acsearthspacechem.1c00204, 2021.

Cai, D., Wang, X., Chen, J., and Li, X.: Molecular Characterization of Organosulfates in Highly Polluted Atmosphere Using Ultra-High-Resolution Mass Spectrometry, J. Geophys. Res.: Atmos. , 125, 10.1029/2019jd032253, 2020.

Chen, Y., Zhang, Y., Lambe, A. T., Xu, R., Lei, Z., Olson, N. E., Zhang, Z., Szalkowski, T., Cui, T., Vizuete, W., Gold, A., Turpin, B. J., Ault, A. P., Chan, M. N., and Surratt, J. D.: Heterogeneous Hydroxyl Radical Oxidation of Isoprene-Epoxydiol-Derived Methyltetrol Sulfates: Plausible Formation Mechanisms of Previously Unexplained Organosulfates in Ambient Fine Aerosols, Environ. Sci. Technol.Lett., 7, 460-468, 10.1021/acs.estlett.0c00276, 2020.

Cui, M., Li, C., Chen, Y., Zhang, F., Li, J., Jiang, B., Mo, Y., Li, J., Yan, C., Zheng, M., Xie, Z., Zhang, G., and Zheng, J.: Molecular characterization of polar organic aerosol constituents in off-road engine emissions using Fourier transform ion cyclotron resonance mass spectrometry (FT-ICR MS): implications for source apportionment, Atmos. Chem. Phys., 19, 13945-13956, 10.5194/acp-19-13945-2019, 2019.

Ding, J., Zhao, P., Su, J., Dong, Q., Du, X., and Zhang, Y.: Aerosol pH and its driving factors in Beijing, Atmos. Chem. Phys., 19, 7939-7954, 10.5194/acp-19-7939-2019, 2019.

Ding, S., Chen, Y., Devineni, S. R., Pavuluri, C. M., and Li, X. D.: Distribution characteristics of organosulfates (OSs) in PM2.5 in Tianjin, Northern China: Quantitative analysis of total and three OS species, Sci. Total. Environ., 834,

641   155314, 10.1016/j.scitotenv.2022.155314, 2022.

642 Estillore, A. D., Hettiyadura, A. P., Qin, Z., Leckrone, E., Wombacher, B., Humphry, T.,

643   Stone, E. A., and Grassian, V. H.: Water Uptake and Hygroscopic Growth of

644   Organosulfate Aerosol, Environ Sci Technol, 50, 4259-4268,

645   10.1021/acs.est.5b05014, 2016.

646 Fabien, P., John, D. C., Henrik, G. K., Andreas, k., Jason, M. S. C., John, H. S., and

647   Paul, O. W.: Unexpected Epoxide Formation in the Gas-Phase Photooxidation

648   of Isoprene, Science, 325, 730-733, 2009.

649 Fleming, L. T., Ali, N. N., Blair, S. L., Roveretto, M., George, C., and Nizkorodov, S.

650   A.: Formation of Light-Absorbing Organosulfates during Evaporation of

651   Secondary Organic Material Extracts in the Presence of Sulfuric Acid, ACS

652   Earth Space Chem., 3, 947-957, 10.1021/acsearthspacechem.9b00036, 2019.

653 Fu, X., Guo, H., Wang, X., Ding, X., He, Q., Liu, T., and Zhang, Z.: PM2.5 acidity at a

654   background site in the Pearl River Delta region in fall-winter of 2007-2012, J.

655   Hazard. Mater., 286, 484-492, 10.1016/j.jhazmat.2015.01.022, 2015.

656 Gani, S., Bhandari, S., Seraj, S., Wang, D. S., Patel, K., Soni, P., Arub, Z., Habib, G.,

657   Hildebrandt Ruiz, L., and Apte, J. S.: Submicron aerosol composition in the

658   world's most polluted megacity: the Delhi Aerosol Supersite study, Atmos.

659   Chem. Phys., 19, 6843-6859, 10.5194/acp-19-6843-2019, 2019.

660 Glasius, M., Thomsen, D., Wang, K., Iversen, L. S., Duan, J., and Huang, R. J.:

661   Chemical characteristics and sources of organosulfates, organosulfonates, and

662   carboxylic acids in aerosols in urban Xi'an, Northwest China, Sci Total Environ,

663   810, 151187, 10.1016/j.scitotenv.2021.151187, 2022.

664 Glasius, M., Bering, M. S., Yee, L. D., de Sa, S. S., Isaacman-VanWertz, G., Wernis, R.

665   A., Barbosa, H. M. J., Alexander, M. L., Palm, B. B., Hu, W., Campuzano-Jost,

666   P., Day, D. A., Jimenez, J. L., Shrivastava, M., Martin, S. T., and Goldstein, A.

667   H.: Organosulfates in aerosols downwind of an urban region in central Amazon,

668   Environ Sci Process Impacts, 20, 1546-1558, 10.1039/c8em00413g, 2018.

669 Guo, H., Xu, L., Bougiatioti, A., Cerully, K. M., Capps, S. L., Hite Jr, J. R., Carlton, A.

670   G., Lee, S. H., Bergin, M. H., Ng, N. L., Nenes, A., and Weber, R. J.: Fine-

671   particle water and pH in the southeastern United States, Atmos. Chem. Phys.,

672   15, 5211-5228, 10.5194/acp-15-5211-2015, 2015.

673 Guo, Q., Wei, Y., and Wan, R.: Leading officials' accountability audit of natural

674   resources and haze pollution: evidence from China, Environmental Science and

675   Pollution Research, 30, 17612-17628, 10.1007/s11356-022-23340-x, 2022.

676 H., J. and Seinfeld, S. N. P.: Atmospheric chemistry and physics: from air pollution to

677   climate change, 2016.

678 Hamilton, J. F., Bryant, D. J., Edwards, P. M., Ouyang, B., Bannan, T. J., Mehra, A.,

679   Mayhew, A. W., Hopkins, J. R., Dunmore, R. E., Squires, F. A., Lee, J. D.,

680   Newland, M. J., Worrall, S. D., Bacak, A., Coe, H., Percival, C., Whalley, L. K.,

681   Heard, D. E., Slater, E. J., Jones, R. L., Cui, T., Surratt, J. D., Reeves, C. E.,

682   Mills, G. P., Grimmond, S., Sun, Y., Xu, W., Shi, Z., and Rickard, A. R.: Key

683   Role of NO_3 Radicals in the Production of Isoprene Nitrates and

684   Nitrooxyorganosulfates in Beijing, Environ. Sci. Technol., 55, 842-853,

10.1021/acs.est.0c05689, 2021.

Hansen, A. M. K., Kristensen, K., Nguyen, Q. T., Zare, A., Cozzi, F., Nøjgaard, J. K., Skov, H., Brandt, J., Christensen, J. H., Ström, J., Tunved, P., Krejci, R., and Glasius, M.: Organosulfates and organic acids in Arctic aerosols: speciation, annual variation and concentration levels, Atmos. Chem. Phys., 14, 7807-7823, 10.5194/acp-14-7807-2014, 2014.

Hawkins, L. N., Russell, L. M., Covert, D. S., Quinn, P. K., and Bates, T. S.: Carboxylic acids, sulfates, and organosulfates in processed continental organic aerosol over the southeast Pacific Ocean during VOCALS-REx 2008, J. Geophys. Res.: Atmos. , 115, 10.1029/2009jd013276, 2010.

Hennigan, C. J., Izumi, J., Sullivan, A. P., Weber, R. J., and Nenes, A.: A critical evaluation of proxy methods used to estimate the acidity of atmospheric particles, Atmos. Chem. Phys., 15, 2775-2790, 10.5194/acp-15-2775-2015, 2015.

Hettiyadura, A. P. S., Al-Naiema, I. M., Hughes, D. D., Fang, T., and Stone, E. A.: Organosulfates in Atlanta, Georgia: anthropogenic influences on biogenic secondary organic aerosol formation, Atmos. Chem. Phys., 19, 3191-3206, 10.5194/acp-19-3191-2019, 2019.

Hettiyadura, A. P. S., Stone, E. A., Kundu, S., Baker, Z., Geddes, E., Richards, K., and Humphry, T.: Determination of atmospheric organosulfates using HILIC chromatography with MS detection, Atoms. Meas. Tech., 8, 2347-2358, 10.5194/amt-8-2347-2015, 2015.

707   Hettiyadura, A. P. S., Jayarathne, T., Baumann, K., Goldstein, A. H., de Gouw, J. A.,

708   Koss, A., Keutsch, F. N., Skog, K., and Stone, E. A.: Qualitative and quantitative

709   analysis of atmospheric organosulfates in Centreville, Alabama, Atmos. Chem.

710   Phys., 17, 1343-1359, 10.5194/acp-17-1343-2017, 2017.

711   Hettiyadura, A. P. S., Xu, L., Jayarathne, T., Skog, K., Guo, H., Weber, R. J., Nenes, A.,

712   Keutsch, F. N., Ng, N. L., and Stone, E. A.: Source apportionment of organic

713   carbon in Centreville, AL using organosulfates in organic tracer-based positive

714   matrix factorization, Atmospheric Environment, 186, 74-88,

715   10.1016/j.atmosenv.2018.05.007, 2018.

716   Hughes, D. D., Christiansen, M. B., Milani, A., Vermeuel, M. P., Novak, G. A., Alwe,

717   H. D., Dickens, A. F., Pierce, R. B., Millet, D. B., Bertram, T. H., Stanier, C. O.,

718   and Stone, E. A.: PM2.5 chemistry, organosulfates, and secondary organic

719   aerosol during the 2017 Lake Michigan Ozone Study, Atmos. Environ., 244,

720   10.1016/j.atmosenv.2020.117939, 2021.

721   Iinuma , Müller , Berndt , Böge , Claeys,, and Herrmann: Evidence for the

722   Existence of Organosulfates from β-Pinene Ozonolysis in Ambient Secondary

723   Organic Aerosol, Environ. Sci. Technol., 41, 6678-6683, 2007.

724   Iinuma, Y., Müller, C., Böge, O., Gnauk, T., and Herrmann, H.: The formation of

725   organic sulfate esters in the limonene ozonolysis secondary organic aerosol

726   (SOA) under acidic conditions, Atmos. Environ., 41, 5571-5583,

727   10.1016/j.atmosenv.2007.03.007, 2007.

728   Jiang, H., Li, J., Tang, J., Cui, M., Zhao, S., Mo, Y., Tian, C., Zhang, X., Jiang, B., Liao,

Y., Chen, Y., and Zhang, G.: Molecular characteristics, sources, and formation pathways of organosulfur compounds in ambient aerosol in Guangzhou, South China, Atmos. Chem. Phys., 22, 6919-6935, 10.5194/acp-22-6919-2022, 2022.

Kanellopoulos, P. G., Kotsaki, S. P., Chrysochou, E., Koukoulakis, K., Zacharopoulos, N., Philippopoulos, A., and Bakeas, E.: PM2.5-bound organosulfates in two Eastern Mediterranean cities: The dominance of isoprene organosulfates, Chemosphere, 297, 134103, 10.1016/j.chemosphere.2022.134103, 2022.

Kourtchev, I., Doussin, J. F., Giorio, C., Mahon, B., Wilson, E. M., Maurin, N., Pangui, E., Venables, D. S., Wenger, J. C., and Kalberer, M.: Molecular composition of fresh and aged secondary organic aerosol from a mixture of biogenic volatile compounds: a high-resolution mass spectrometry study, Atmos. Chem. Phys., 15, 5683-5695, 10.5194/acp-15-5683-2015, 2015.

Kristensen, K. and Glasius, M.: Organosulfates and oxidation products from biogenic hydrocarbons in fine aerosols from a forest in North West Europe during spring, Atmos. Environ., 45, 4546-4556, 10.1016/j.atmosenv.2011.05.063, 2011.

Li, X., Zhang, Y., Shi, L., Kawamura, K., Kunwar, B., Takami, A., Arakaki, T., and Lai, S.: Aerosol Proteinaceous Matter in Coastal Okinawa, Japan: Influence of Long-Range Transport and Photochemical Degradation, Environ Sci Technol, 56, 5256-5265, 10.1021/acs.est.1c08658, 2022.

Menon, S., ;, Unger, N., ;, Koch, D., ;, Francis, J., ;, Garrett, T., ;, Sednev, I., ;, Shindell, D., ;, and Streets, D., ;: Aerosol climate effects and air quality impacts from 1980 to 2030, Environ. Res. Lett., 3, 10.1088/1748-9326/3/2/024004, 2008.

Nestorowicz, K., Jaoui, M., Rudzinski, K. J., Lewandowski, M., Kleindienst, T. E., Spolnik, G., Danikiewicz, W., and Szmigielski, R.: Chemical composition of isoprene SOA under acidic and non-acidic conditions: effect of relative humidity, Atmos Chem Phys, 18, 18101-18121, 10.5194/acp-18-18101-2018, 2018.

Nguyen, Q. T., Christensen, M. K., Cozzi, F., Zare, A., Hansen, A. M. K., Kristensen, K., Tulinius, T. E., Madsen, H. H., Christensen, J. H., Brandt, J., Massling, A., Nøjgaard, J. K., and Glasius, M.: Understanding the anthropogenic influence on formation of biogenic secondary organic aerosols in Denmark via analysis of organosulfates and related oxidation products, Atmos. Chem. Phys., 14, 8961-8981, 10.5194/acp-14-8961-2014, 2014.

Nguyen, T. B., Bates, K. H., Crounse, J. D., Schwantes, R. H., Zhang, X., Kjaergaard, H. G., Surratt, J. D., Lin, P., Laskin, A., Seinfeld, J. H., and Wennberg, P. O.: Mechanism of the hydroxyl radical oxidation of methacryloyl peroxynitrate (MPAN) and its pathway toward secondary organic aerosol formation in the atmosphere, Phys. Chem. Chem. Phys., 17, 17914-17926, 10.1039/c5cp02001h, 2015.

Nozière, B., Ekström, S., Alsberg, T., and Holmström, S.: Radical-initiated formation of organosulfates and surfactants in atmospheric aerosols, Geophys. Res. Lett., 37, n/a-n/a, 10.1029/2009gl041683, 2010.

O'Brien, R. E., Laskin, A., Laskin, J., Rubitschun, C. L., Surratt, J. D., and Goldstein, A. H.: Molecular characterization of S- and N-containing organic constituents

in ambient aerosols by negative ion mode high-resolution Nanospray Desorption Electrospray Ionization Mass Spectrometry: CalNex 2010 field study, Journal of Geophysical Research: Atmospheres, 119, 10.1002/2014jd021955, 2014.

Olson, C. N., Galloway, M. M., Yu, G., Hedman, C. J., Lockett, M. R., Yoon, T., Stone, E. A., Smith, L. M., and Keutsch, F. N.: Hydroxycarboxylic acid-derived organosulfates: synthesis, stability, and quantification in ambient aerosol, Environ Sci Technol, 45, 6468-6474, 10.1021/es201039p, 2011.

Passananti, M., Kong, L., Shang, J., Dupart, Y., Perrier, S., Chen, J., Donaldson, D. J., and George, C.: Organosulfate Formation through the Heterogeneous Reaction of Sulfur Dioxide with Unsaturated Fatty Acids and Long-Chain Alkenes, Angew. Chem. Int. Ed. Engl., 55, 10336-10339, 10.1002/anie.201605266, 2016.

Paulson, S. E. and Orlando, J. J.: The reactions of ozone with alkenes: An important source of HOxin the boundary layer, Geophys. Res. Lett., 23, 3727-3730, 10.1029/96gl03477, 1996.

Pei, Z., Chen, X., Li, X., Liang, J., Lin, A., Li, S., Yang, S., Bin, J., and Dai, S.: Impact of macroeconomic factors on ozone precursor emissions in China, Journal of Cleaner Production, 344, 10.1016/j.jclepro.2022.130974, 2022.

Ramanathan , V., Crutzen, P. J., Kiehl, J. T., and Rosenfeld, D.: Aerosols, Climate, and the Hydrological Cycle, Science, 294, 2119-2124, 2001.

Riva, M., Budisulistiorini, S. H., Zhang, Z., Gold, A., and Surratt, J. D.: Chemical characterization of secondary organic aerosol constituents from isoprene

795 ozonolysis in the presence of acidic aerosol, Atmospheric Environment, 130, 5-

796 13, 10.1016/j.atmosenv.2015.06.027, 2016a.

797 Riva, M., Da Silva Barbosa, T., Lin, Y.-H., Stone, E. A., Gold, A., and Surratt, J. D.:

798 Chemical characterization of organosulfates in secondary organic aerosol

799 derived from the photooxidation of alkanes, Atmos. Chem. Phys., 16, 11001-

800 11018, 10.5194/acp-16-11001-2016, 2016b.

801 Riva, M., Tomaz, S., Cui, T., Lin, Y. H., Perraudin, E., Gold, A., Stone, E. A., Villenave,

802 E., and Surratt, J. D.: Evidence for an unrecognized secondary anthropogenic

803 source of organosulfates and sulfonates: gas-phase oxidation of polycyclic

804 aromatic hydrocarbons in the presence of sulfate aerosol, Environ. Sci. Technol.,

805 49, 6654-6664, 10.1021/acs.est.5b00836, 2015.

806 Riva, M., Chen, Y., Zhang, Y., Lei, Z., Olson, N. E., Boyer, H. C., Narayan, S., Yee, L.

807 D., Green, H. S., Cui, T., Zhang, Z., Baumann, K., Fort, M., Edgerton, E.,

808 Budisulistiorini, S. H., Rose, C. A., Ribeiro, I. O., RL, E. O., Dos Santos, E. O.,

809 Machado, C. M. D., Szopa, S., Zhao, Y., Alves, E. G., de Sa, S. S., Hu, W.,

810 Knipping, E. M., Shaw, S. L., Duvoisin Junior, S., de Souza, R. A. F., Palm, B.

811 B., Jimenez, J. L., Glasius, M., Goldstein, A. H., Pye, H. O. T., Gold, A., Turpin,

812 B. J., Vizuete, W., Martin, S. T., Thornton, J. A., Dutcher, C. S., Ault, A. P., and

813 Surratt, J. D.: Increasing Isoprene Epoxydiol-to-Inorganic Sulfate Aerosol Ratio

814 Results in Extensive Conversion of Inorganic Sulfate to Organosulfur Forms:

815 Implications for Aerosol Physicochemical Properties, Environ. Sci. Technol., 53,

816 8682-8694, 10.1021/acs.est.9b01019, 2019.

817   Schindelka, J., Iinuma, Y., Hoffmann, D., and Herrmann, H.: Sulfate radical-initiated

818   formation of isoprene-derived organosulfates in atmospheric aerosols, Faraday

819   Discuss., 165, 237-259, 10.1039/c3fd00042g, 2013.

820   Shalamzari, M. S., Ryabtsova, O., Kahnt, A., Vermeylen, R., Herent, M. F., Quetin-

821   Leclercq, J., Van der Veken, P., Maenhaut, W., and Claeys, M: Mass

822   spectrometric characterization of organosulfates related to secondary organic

823   aerosol from isoprene, Rapid Commun. Mass Spectrom., 784-794,

824   10.1002/rcm.6511, 2013, 2013.

825   Shang, J., Passananti, M., Dupart, Y., Ciuraru, R., Tinel, L., Rossignol, S., Perrier, S.,

826   Zhu, T., and George, C.: SO2 Uptake on Oleic Acid: A New Formation Pathway

827   of Organosulfur Compounds in the Atmosphere, Environ. Sci. Technol.Lett., 3,

828   67-72, 10.1021/acs.estlett.6b00006, 2016.

829   Staudt, S., Kundu, S., Lehmler, H. J., He, X., Cui, T., Lin, Y. H., Kristensen, K., Glasius,

830   M., Zhang, X., Weber, R. J., Surratt, J. D., and Stone, E. A.: Aromatic

831   organosulfates in atmospheric aerosols: synthesis, characterization, and

832   abundance, Atmos Environ (1994), 94, 366-373,

833   10.1016/j.atmosenv.2014.05.049, 2014.

834   Stone, E. A., Yang, L., Yu, L. E., and Rupakheti, M.: Characterization of organosulfates

835   in atmospheric aerosols at Four Asian locations, Atmos. Environ., 47, 323-329,

836   10.1016/j.atmosenv.2011.10.058, 2012.

837   Surratt, J. D., Lewandowski, M., Offenberg, J. H., Jaoui, M., Kleindienst, T.E., Edney,

838   E. O., and Seinfeld, J. H.: Effect of Acidity on Secondary Organic Aerosol

Formation from Isoprene, Environ. Sci. Technol., 41, 5363–5369, 2007a.

Surratt, J. D., Chan, A. W., Eddingsaas, N. C., Chan, M., Loza, C. L., Kwan, A. J., Hersey, S. P., Flagan, R. C., Wennberg, P. O., and Seinfeld, J. H.: Reactive intermediates revealed in secondary organic aerosol formation from isoprene, Proc. Natl. Acad. Sci. U.S.A., 107, 6640-6645, 10.1073/pnas.0911114107, 2010.

Surratt, J. D., Kroll, J. H., Kleindienst, T. E., Edney, E. O., Claeys, M., Sorooshian, A., Ng, N. L., Offenberg, J. H., Lewandowski, M., Jaoui, M., Flagan, R. C., and Seinfeld, J. H.: Evidence for Organosulfates in Secondary Organic Aerosol, Environ. Sci. Technol., 41, 517–527, 2007b.

Surratt, J. D., Gómez-González, Y., Chan, A. W. H., Vermeylen, R., Shahgholi, M., Kleindienst, T. E., Edney, E. O., Offenberg, J. H., Lewandowski, M., Jaoui, M., Maenhaut, W., Claeys, M., Flagan, R. C., and Seinfeld, J. H.: Organosulfate Formation in Biogenic Secondary Organic Aerosol, J. Phys. Chem. A., 112, 8345-8378, 10.1021/jp802310p, 2008.

Tolocka, M. P. and Turpin, B.: Contribution of organosulfur compounds to organic aerosol mass, Environ. Sci. Technol., 46, 7978-7983, 10.1021/es300651v, 2012.

Turpin, B. J. and Lim, H.-J.: Species Contributions to PM2.5 Mass Concentrations: Revisiting Common Assumptions for Estimating Organic Mass, Aerosol Sci.Technol., 35, 602-610, 10.1080/02786820119445, 2001.

Wach, P., Spolnik, G., Rudzinski, K. J., Skotak, K., Claeys, M., Danikiewicz, W., and Szmigielski, R.: Radical oxidation of methyl vinyl ketone and methacrolein in aqueous droplets: Characterization of organosulfates and atmospheric

861   implications, Chemosphere, 214, 1-9, 10.1016/j.chemosphere.2018.09.026,

862   2019.

863   Wang, Y., Ren, J., Huang, X. H. H., Tong, R., and Yu, J. Z.: Synthesis of Four

864   Monoterpene-Derived Organosulfates and Their Quantification in Atmospheric

865   Aerosol Samples, Environ. Sci. Technol., 51, 6791-6801,

866   10.1021/acs.est.7b01179, 2017.

867   Wang, Y., Ma, Y., Kuang, B., Lin, P., Liang, Y., Huang, C., and Yu, J. Z.: Abundance of

868   organosulfates derived from biogenic volatile organic compounds: Seasonal and

869   spatial contrasts at four sites in China, Sci. Total. Environ., 806, 151275,

870   10.1016/j.scitotenv.2021.151275, 2022.

871   Wang, Y., Zhao, Y., Wang, Y., Yu, J. Z., Shao, J., Liu, P., Zhu, W., Cheng, Z., Li, Z., Yan,

872   N., and Xiao, H.: Organosulfates in atmospheric aerosols in Shanghai, China:

873   seasonal and interannual variability, origin, and formation mechanisms, Atmos.

874   Chem. Phys., 21, 2959-2980, 10.5194/acp-21-2959-2021, 2021.

875   Wang, Y., Hu, M., Wang, Y.-C., Li, X., Fang, X., Tang, R., Lu, S., Wu, Y., Guo, S., Wu,

876   Z., Hallquist, M., and Yu, J. Z.: Comparative Study of Particulate

877   Organosulfates in Contrasting Atmospheric Environments: Field Evidence for

878   the Significant Influence of Anthropogenic Sulfate and NOx, Environ. Sci.

879   Technol.Lett., 7, 787-794, 10.1021/acs.estlett.0c00550, 2020.

880   Wang, Y., Hu, M., Guo, S., Wang, Y., Zheng, J., Yang, Y., Zhu, W., Tang, R., Li, X., Liu,

881   Y., Le Breton, M., Du, Z., Shang, D., Wu, Y., Wu, Z., Song, Y., Lou, S., Hallquist,

882   M., and Yu, J.: The secondary formation of organosulfates under interactions

883  between biogenic emissions and anthropogenic pollutants in summer in Beijing,

884  Atmos. Chem. Phys., 18, 10693-10713, 10.5194/acp-18-10693-2018, 2018.

885 Xu, Y., Miyazaki, Y., Tachibana, E., Sato, K., Ramasamy, S., Mochizuki, T., Sadanaga,

886  Y., Nakashima, Y., Sakamoto, Y., Matsuda, K., and Kajii, Y.: Aerosol Liquid

887  Water Promotes the Formation of Water-Soluble Organic Nitrogen in

888  Submicrometer Aerosols in a Suburban Forest, Environ. Sci. Technol., 54,

889  1406-1414, 10.1021/acs.est.9b05849, 2020.

890 Yassine, M. M., Dabek-Zlotorzynska, E., Harir, M., and Schmitt-Kopplin, P.:

891  Identification of weak and strong organic acids in atmospheric aerosols by

892  capillary electrophoresis/mass spectrometry and ultra-high-resolution Fourier

893  transform ion cyclotron resonance mass spectrometry, Anal. Chem., 84, 6586-

894  6594, 10.1021/ac300798g, 2012.

895 Ye, J., Abbatt, J. P. D., and Chan, A. W. H.: Novel pathway of SO2 oxidation in the

896  atmosphere:reactions with monoterpene ozonolysis intermediates and

897  secondary organic aerosol, Atmos. Chem. Phys., 18, 5549-5565, 10.5194/acp-

898  18-5549-2018, 2018.

899

900

901

902

903

904
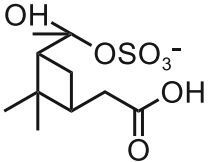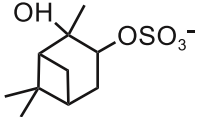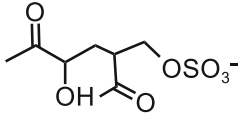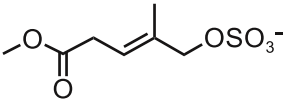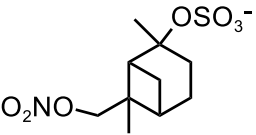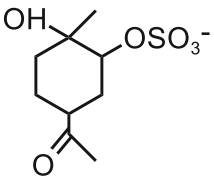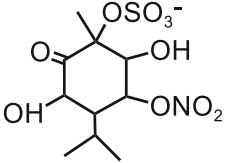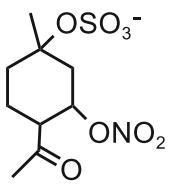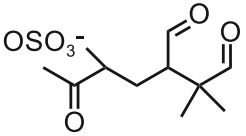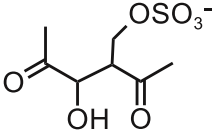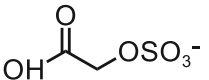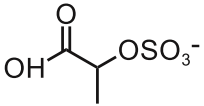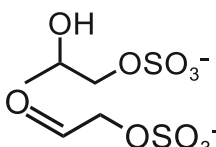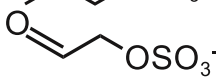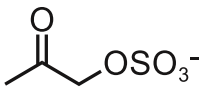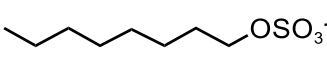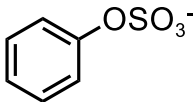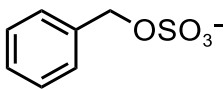
Table 1. Organosulfate quantification using UPLC-ESI(-)-QToFMS(/MS).

Formula[a]	MW (Da)	Standard	Structure	Reference
Isoprene-derived OSs ($n = 12$)				
$C_4H_7O_7S^-$	198.9912	Lactic acid sulfate (LAS)		(Hettiyadura et al. 2015)
$C_5H_{11}O_6S^-$	199.0276	LAS		(Riva et al. 2016a)
$C_5H_9O_7S^-$	213.0069	LAS		(Riva et al. 2016a)
$C_4H_7O_5S^-$	167.0014	LAS		(Schindelka et al. 2013)
$C_4H_7O_6S^-$	182.9963	LAS		(Shalamzari 2013)
$C_5H_7O_7S^-$	210.9912	LAS		(Hettiyadura et al. 2015)
$C_5H_9O_6S^-$	197.0120	LAS		(Riva et al. 2016a)
$C_5H_{10}NO_9S^-$	260.0076	LAS		(Surratt et al. 2007a)
$C_7H_9O_7S^-$	237.0069	LAS		(Nozière et al. 2010)
$C_5H_8NO_{10}S^-$	273.9869	LAS		(Nestorowicz et al. 2018)
$C_5H_{10}NO_9S^-$	260.0076	LAS		(Surratt et al. 2007a)
$C_5H_{11}O_7S^-$	215.0225	LAS		(Surratt et al. 2010)

Other quantified isoprene-derived OSs were shown in **SI**

Monoterpene-derived OSs ($n = 10$)

Formula	m/z	Name	Structure	Reference
$C_{10}H_{17}O_7S^-$	281.0695	α-Pinene sulfate		(Nozière et al. 2010)
$C_{10}H_{17}O_5S^-$	249.0797	α-Pinene sulfate		(Wang et al. 2017)
$C_8H_{13}O_7S^-$	253.0382	Glycolic acid sulfate (GAS)		(Schindelka et al. 2013)
$C_7H_{11}O_6S^-$	223.0276	GAS		(Yassine et al. 2012)
$C_{10}H_{16}NO_7S^-$	294.0647	α-Pinene sulfate		(Surratt et al. 2008)
$C_9H_{15}O_6S^-$	251.0589	Limonaketone sulfate		(Wang et al. 2017)
$C_{10}H_{16}NO_{10}S^-$	342.0495	Limonaketone sulfate		(Yassine et al. 2012)
$C_9H_{14}NO_8S^-$	296.0440	Limonaketone sulfate		(Surratt et al. 2008)
$C_{10}H_{15}O_7S^-$	279.0538	GAS		(Surratt et al. 2007a)
$C_7H_{11}O_7S^-$	239.0225	GAS		(Nozière et al. 2010)

Other quantified monoterpene-derived OSs were shown in **SI**

C₂-C₃ OSs (*n* = 6)

$C_3H_5O_4S^-$	136.9909	GAS	unknown	(Yassine et al.
$C_2H_3O_6S^-$	154.9650	GAS		(Olson et al. 2011)

Formula	m/z	Name	Structure	Reference
$C_3H_5O_6S^-$	168.9807	LAS		(Olson et al. 2011)
$C_3H_7O_5S^-$	155.0014	GAS		(Hettiyadura et al. 2019)
$C_2H_3O_5S^-$	138.9701	GAS		(Yassine et al. 2012)
$C_3H_5O_5S^-$	152.9858	GAS		(Hettiyadura et al. 2015)

OSa (aliphatic-OSs) ($n = 1$)

Formula	m/z	Name	Structure	Reference
$C_8H_{17}O_4S^-$	210.0926	Sodium octyl Sulfate (SOS)		(Wang et al. 2021)

Other quantified aliphatic-derived OSs were shown in **SI**

OSa (aromatic-OSs) ($n = 2$)

Formula	m/z	Name	Structure	Reference
$C_6H_5O_4S^-$	172.9909	Phenyl sulfate		(Wang et al. 2021)
$C_7H_7SO_4S^-$	218.9786	Phenyl sulfate		(Wang et al. 2021)

Other quantified aromatic-derived OSs were shown in **SI**

OS$_a$-other ($n =3$)

Formula	m/z	Name	Structure	Reference
$C_4H_7O_4S^-$	151.0065	Methyl sulfate	unknown	(Wang et al. 2021)
$C_5H_7O_6S^-$	194.9963	GAS	unknown	(Wang et al. 2021)
$C_6H_9O_6S^-$	209.0120	GAS	unknown	(Berndt et al. 2016)

906   [a] MS/MS data supports tentative structural identification based on the listed references.

907

908

909

910

911

912

913

914 **Figure 1.**
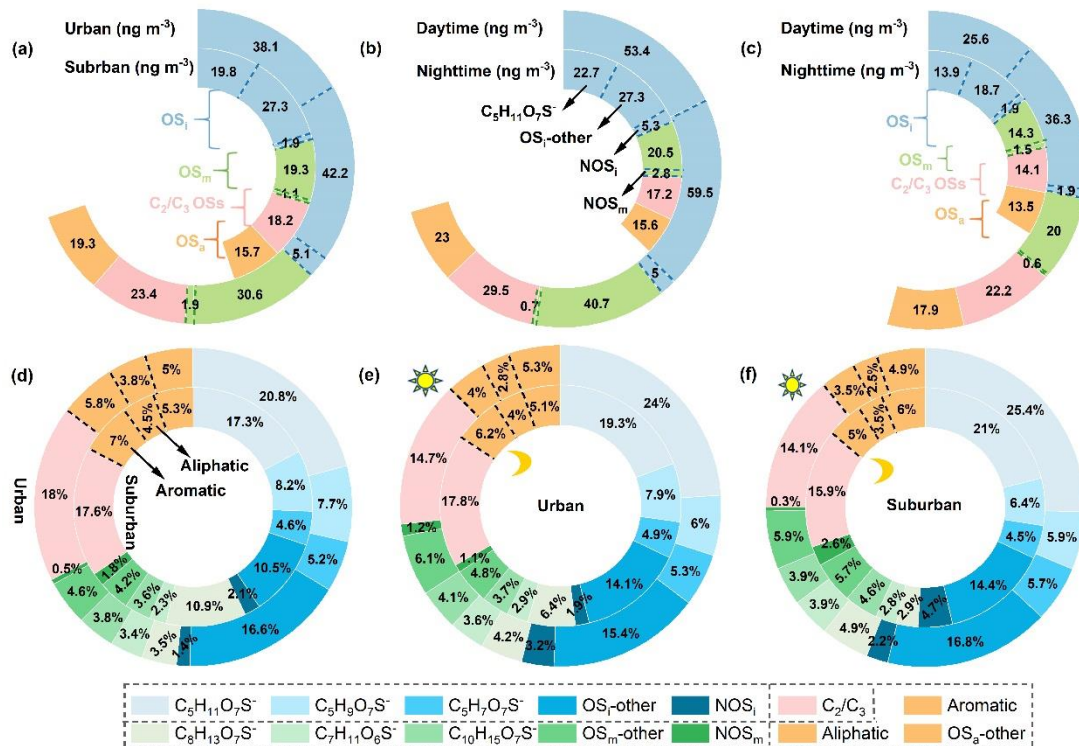
915

916 **Figure 1.** Average distributions in the mass concentrations and mass fractions of

917 various OSs in $PM_{2.5}$ in different cases: (a–d) urban vs suburban for all data, (b–e)

918 daytime vs nighttime in the urban area, as well as (c–f) daytime vs nighttime in the

919 suburban area. The areas divided by dashed lines in Figures a-c indicate $C_5H_{11}O_7S^-$,

920 $OS_{i\text{-other}}$, NOS_i, and NOS_m in sequence, as illustrated in Figure b. The areas divided by

921 dashed lines in Figures d-f indicate aromatic and aliphatic OSs in sequence, as

922 illustrated in Figure d.

923

924

925

926 **Figure 2.**
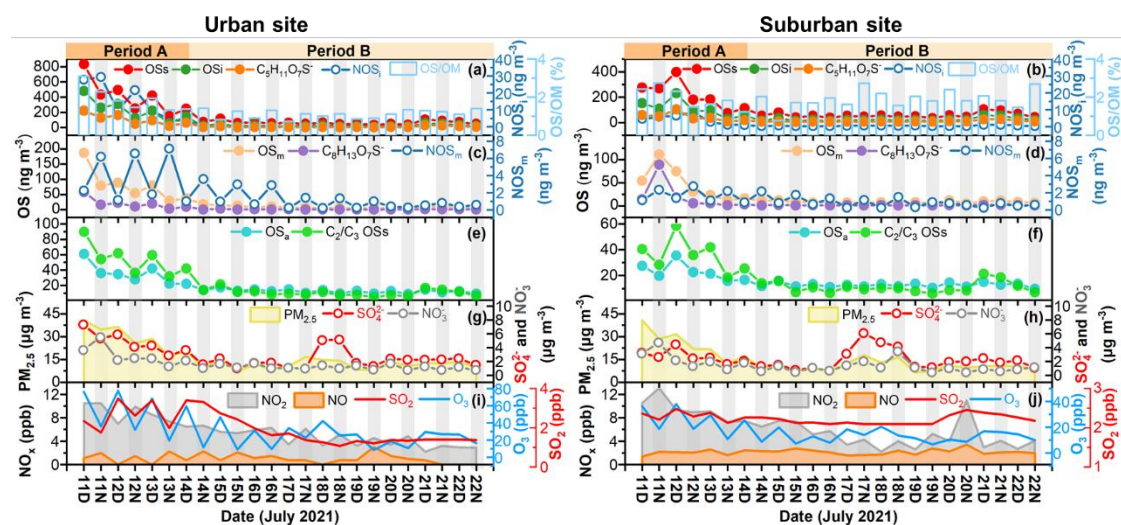
927

928 **Figure 2.** Temporal variations of OSs and other chemical components in PM$_{2.5}$ as well

929 as other data measured in urban and suburban Shanghai in summer. (a–b) OSs, OS$_i$,

930 C$_5$H$_{11}$O$_7$S$^-$ (major OS$_i$ species), NOS$_i$, and OS/OM (%); (c–d) OS$_m$, C$_8$H$_{13}$O$_7$S$^-$, and

931 NOS$_m$; (e–f) OS$_a$ and C$_2$-C$_3$ OSs; (g–h) PM$_{2.5}$, SO$_4^{2-}$, and NO$_3^-$; and (i–j) NO$_2$, NO, SO$_2$,

932 and O$_3$. The sampling period A and B indicate the relatively polluted period and the

933 clean period, respectively.

934

935 **Figure 3.**

936
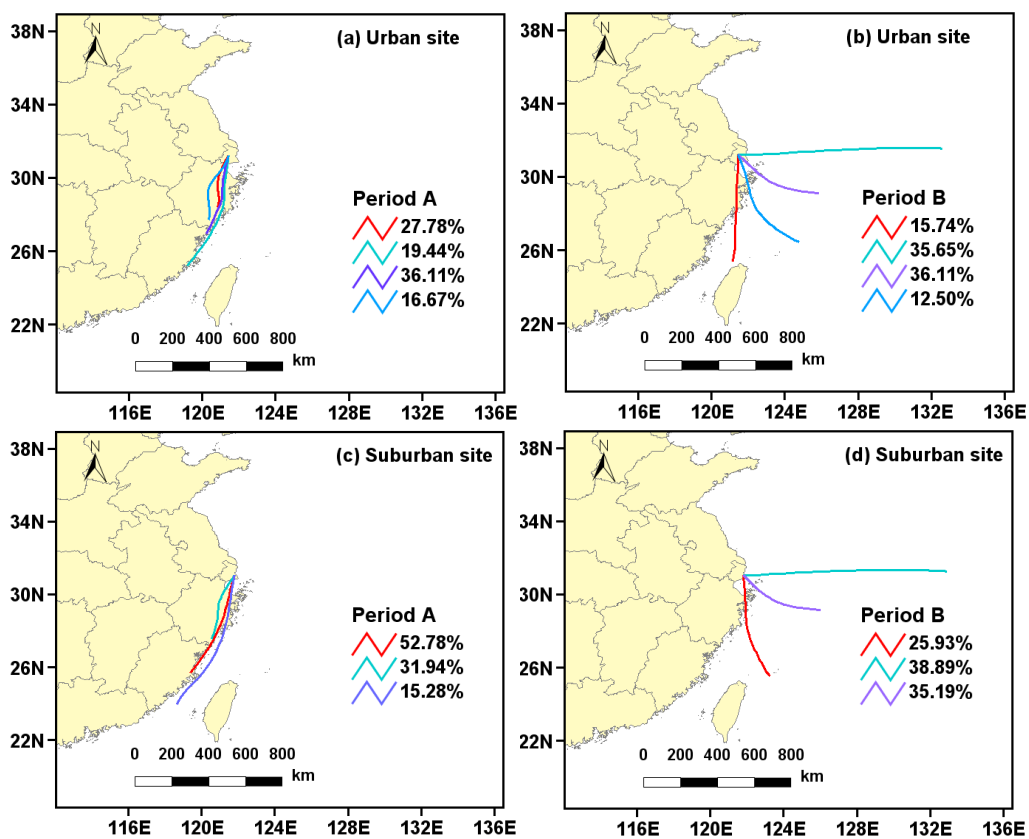
937
938

939 **Figure 3.** Air mass backward trajectories of the major clusters in different periods in

940 the (a–b) urban and (c–d) suburban areas.

941
942

943 **Figure 4.**

944
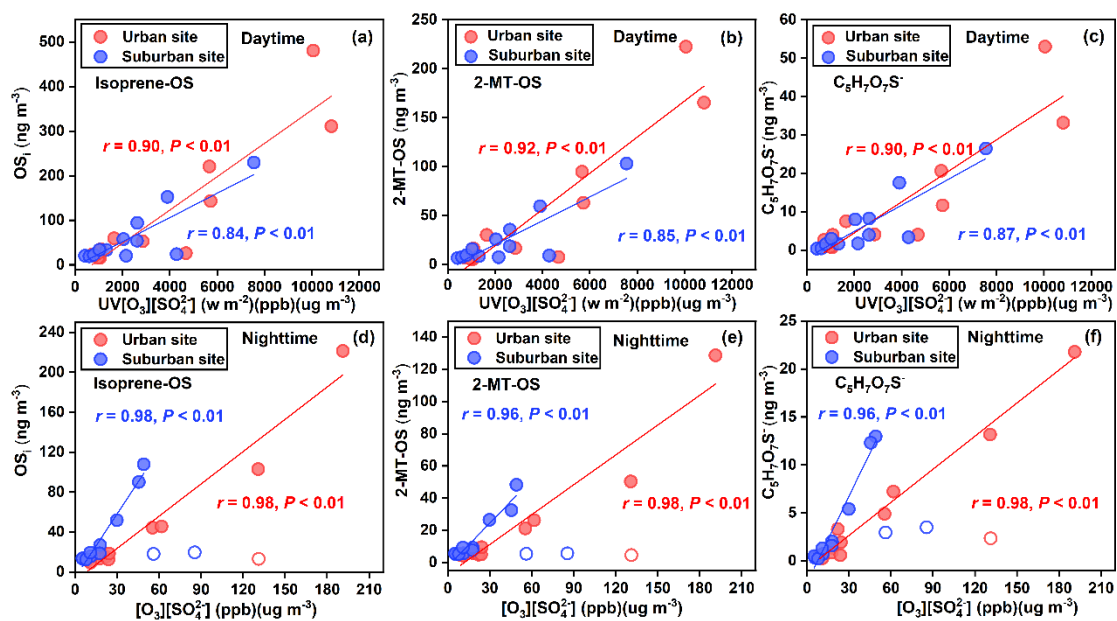
945

946 **Figure 4.** Mass concentrations of (a and d) OS_i, (b and e) 2-MT-OS, and (c and f)

947 $C_5H_7O_7S^-$ as functions of $UV[O_3][SO_4^{2-}]$ and $[O_3][SO_4^{2-}]$ during daytime and nighttime

948 in the urban (red solid circles) and suburban sites (blue solid circles). The open circles

949 represent outliers, which was attributed to several particularly high sulfate events.

950

951 **Figure 5.**
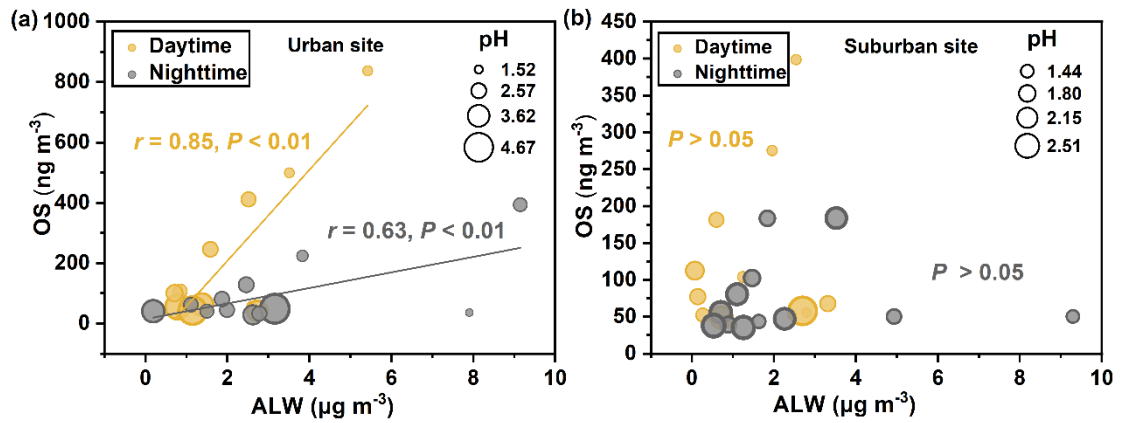
952

953 **Figure 5.** Scatterplots of the ALW concentrations with the mass concentrations of total

954 OSs in PM$_{2.5}$ collected in the (a) urban and (b) suburban areas. Yellow and grey lines

955 show regression lines in the daytime and nighttime, respectively.

956
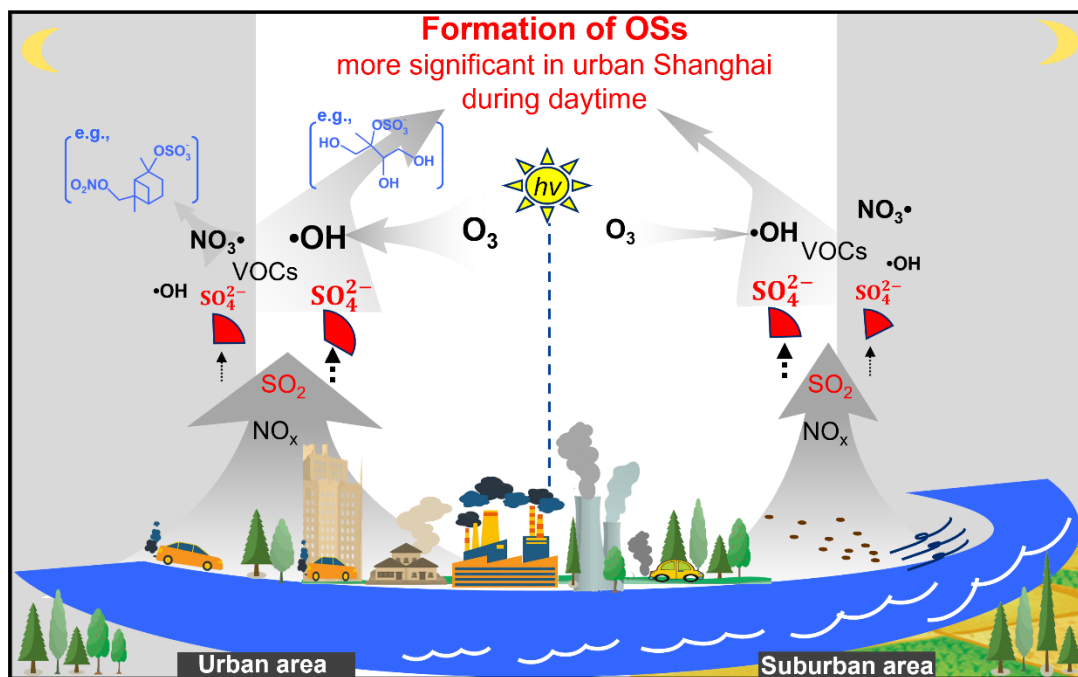
957

958 **Figure 6.** Conceptual picture showing the characteristic and atmospheric process of

959 OSs in urban and suburban Shanghai.

960